


Research Article

Stochastic Optimization of a Nonlinear Base Isolation System with LRB and EIMD for Building Structures

Heng Wang,¹ Wenai Shen ,^{1,2} Hongping Zhu,^{1,2} and Hui Luo¹

¹School of Civil and Hydraulic Engineering, Huazhong University of Science and Technology, Wuhan 430074, China

²Hubei Key Laboratory of Control Structure, Huazhong University of Science and Technology, Wuhan 430074, China

Correspondence should be addressed to Wenai Shen; wshen@hust.edu.cn

Received 14 October 2022; Revised 7 January 2023; Accepted 17 January 2023; Published 7 February 2023

Academic Editor: Zili Zhang

Copyright © 2023 Heng Wang et al. This is an open access article distributed under the Creative Commons Attribution License, which permits unrestricted use, distribution, and reproduction in any medium, provided the original work is properly cited.

Base-isolated structures achieve superior seismic performance but with the cost of large deformation of the base floor, which possibly causes superstructure collapse during severe earthquakes. Hence, it is of great interest to develop hybrid base isolation systems that can reduce the base deformation and simultaneously improve the superstructure's performance. Recently, several hybrid base isolation systems using inerter-based dampers have emerged; however, the nonlinear performance of the isolators has rarely been considered in these studies. In this paper, we conduct a nonlinear stochastic optimization of a novel hybrid base isolation system with lead-rubber bearings (LRB) and electromagnetic inertial mass dampers (EIMD). Based on the Bouc–Wen hysteretic model of the LRB, we derive the semianalytical solutions of the response variances of a simplified base-isolated model subjected to stationary seismic excitations. Then, based on the semianalytical solutions, we propose a procedure for optimizing the EIMD aimed at minimizing the superstructure interstory drift. In addition, we investigate the effect of site conditions and postyielding to preyielding stiffness ratios of the LRB on the optimal EIMD parameters and corresponding seismic performance. It is found that the hybrid base isolation system achieves better performance at a soft site than at a firm site. Results of a hybrid base-isolated building under artificial and real earthquake excitations illustrate that the EIMD can reduce both the base deformation and superstructure response, which outperforms the hybrid base-isolated building with conventional viscous dampers (VD).

1. Introduction

Base isolation technology can effectively protect civil structures from damage induced by earthquake ground motions, the principle of which is to shift the fundamental period of the isolated structure away from the frequency range with the strongest seismic input energy, so the ground motion will not be transmitted into the structure [1]. In engineering practice, different types of base isolation systems, such as lead-rubber bearings (LRB) [2, 3], sliding isolation bearings [4], and friction pendulum systems (FPS) [5, 6], have been widely applied in base-isolated structures (BIS). Although the original structure response is greatly reduced, a large deformation induced by the earthquake ground motion will occur on the base floor, thus the superstructure might face collapse risk when experiencing an extremely rare earthquake. Hence, hybrid base isolation systems, which combine isolation bearings and passive

dampers, receive increasing attention [7–11] and intend to tackle the challenges of overlage base deformation of the BIS during extremely rare earthquakes while maintaining or reducing superstructure responses.

In a hybrid base isolation system, the supplemental passive damper plays a key role. In the 1990s, Kelly et al. proposed a classical hybrid base isolation system using fluid viscous dampers, which is capable of providing properly designed damping to enhance the seismic performance of the BIS [12]. In the past decade, inerter-based dampers have received increasing attention in the development of hybrid base isolation systems. Different from fluid viscous dampers, inerter-based dampers not only provide damping force but also inertial force. Due to the inertial force, inerter-based dampers can prolong the period of the BIS and alter the mode shapes, etc., which may be beneficial for seismic response control if properly designed [13].

To date, the studies on hybrid base isolation systems with inerter-based dampers can be categorized into two types: linear analysis and nonlinear analysis. In the linear analysis, both isolation bearings, inerter-based dampers, and superstructures are assumed to respond linearly. According to linear mechanical models, the inerter-based dampers can be classified into a total of five types: viscous mass damper (VMD) [14, 15] (or electromagnetic inertial mass damper (EIMD) [16], tuned viscous mass damper (TVMD) [14], tuned inerter mass (TID) [17], tuned mass damper-inerter (TMDI) [18], and tuned inertial mass electromagnetic damper (TIMED) [19]. The simplest case is to add a single inerter to the BIS. The second modal response can be eliminated if the inerter is properly designed [20]. Other studies reveal, however, that the inerter may increase the acceleration responses of the superstructure [21]. The authors investigated the hybrid base isolation system with the EIMD and found that the EIMD can limit the base floor deformation and reduce the superstructure responses at the same time, which performs better in soft soil conditions than in firm soil conditions [13, 22]. Due to the filter function of the supplemental spring in series with the VMD, it is found that the TVMD can further improve the superstructure acceleration control performance in contrast to the VMD [23, 24]. In addition, the hybrid base isolation system with the TID has been extensively studied [25, 26], which found that the TID performs well in soft soil conditions [27].

It is of great interest to investigate the nonlinear performance of hybrid base isolation systems because the force-deformation behaviors of base isolation systems are highly nonlinear. Recently, the nonlinear analysis of the hybrid base isolation system with inerter-based dampers has drawn increasing attention [28–30]. In 2018, De Domenico et al. [28] investigated the hybrid base isolation system composed of LRB/FPS and the TMDI, which demonstrated the robustness and good performance of the system. Zhao et al. [29] compared the performance of the FPS with the TID or the TVMD and found that the former has better control performance. Considering the nonlinear model of the LRB, Li et al. [30] illustrated that TMDI has superior control performance under near-fault pulse-type earthquakes compared with TMD. However, there are few pieces of literature on the nonlinear analysis and optimization of the hybrid base isolation system with the EIMD [31]. Although the linear analysis has demonstrated the salient feature of the hybrid base isolation system with the EIMD, its parameter optimization and actual seismic performance when considering the nonlinear behavior of the LRB have not been reported yet.

To address the above issue, we conduct a stochastic optimization of a nonlinear hybrid base isolation system consisting of an LRB and an EIMD. The semianalytical solutions of the response variances of the nonlinear hybrid base isolation system are derived under the Kanai-Tajimi filtered Gaussian white-noise process. Based on the

solutions, we then propose a stochastic optimization procedure for the EIMD design. Particularly, we investigate the optimal parameters of the EIMD and corresponding seismic response reduction performance considering the LRB with different ratios of postyielding to preyielding stiffness under firm and soft soil conditions. The effectiveness of the proposed stochastic optimization procedure is then verified using a numerical example of a seven-story nonlinear BIS subjected to both a set of stationary artificial excitations and real ground motion records.

2. Nonlinear Stochastic Analysis of Hybrid Base Isolation Systems

2.1. Motion Equations. This section carries out a stochastic analysis of a hybrid base isolation system consisting of an LRB and an EIMD. As depicted in Figure 1(a), a BIS with the hybrid base isolation system is simplified to a two-degree-of-freedom (2-DOF) dynamical system. Figure 1(b) shows the configuration of the EIMD, whose detailed design and mechanical model can be referred to in our previous study [16].

In this study, the mechanical behavior of the LRB is simulated by the Bouc–Wen hysteretic model (Figure 1(c)) and the linear damper model, and its restoring force is given by [3]

$$F_{\text{LRB}}(v_b, \dot{v}_b, Z) = c_b \dot{v}_b + \alpha k_b v_b + (1 - \alpha) k_b v_{yb} Z, \quad (1)$$

where c_b and k_b denote the viscous damping and initial stiffness of the LRB, respectively; α is the ratio of postyielding to preyielding stiffness of the bearing; v_{yb} is the yield displacement of the bearing; Z is a dimensionless hysteretic variable that satisfies the equation

$$v_{yb} \dot{Z} = A \dot{v}_b - \gamma |\dot{v}_b| |Z|^{\eta-1} Z - \beta \dot{v}_b |Z|^\eta, \quad (2)$$

in which the nondimensional parameters A , γ , β , and η are related to the shape and smoothness of the hysteresis loops.

Figure 1(d) shows the linearized mechanical model of the EIMD [16]; the resisting force of the EIMD is given by

$$F_{\text{EIMD}}(\dot{v}_b, \ddot{v}_b) = m_e \ddot{v}_b + c_d \dot{v}_b. \quad (3)$$

The linearized model of the EIMD was validated in our previous study [16]. As shown in Figure 2, the predicted hysteretic curve using equation (3) matches well with the measured counterpart, illustrating the validity of the linearized model.

The equations of motion of the 2-DOF dynamical system subjected to seismic excitation \ddot{u}_g are given by

$$m_s \ddot{v}_s + m_s \ddot{v}_b + c_s \dot{v}_s + k_s v_s = -m_s \ddot{u}_g, \quad (4a)$$

$$\begin{aligned} m_s \ddot{v}_s + (m_s + m_b) \ddot{v}_b + F_{\text{EIMD}}(\dot{v}_b, \ddot{v}_b) \\ + F_{\text{LRB}}(v_b, \dot{v}_b, Z) = -(m_s + m_b) \ddot{u}_g. \end{aligned} \quad (4b)$$

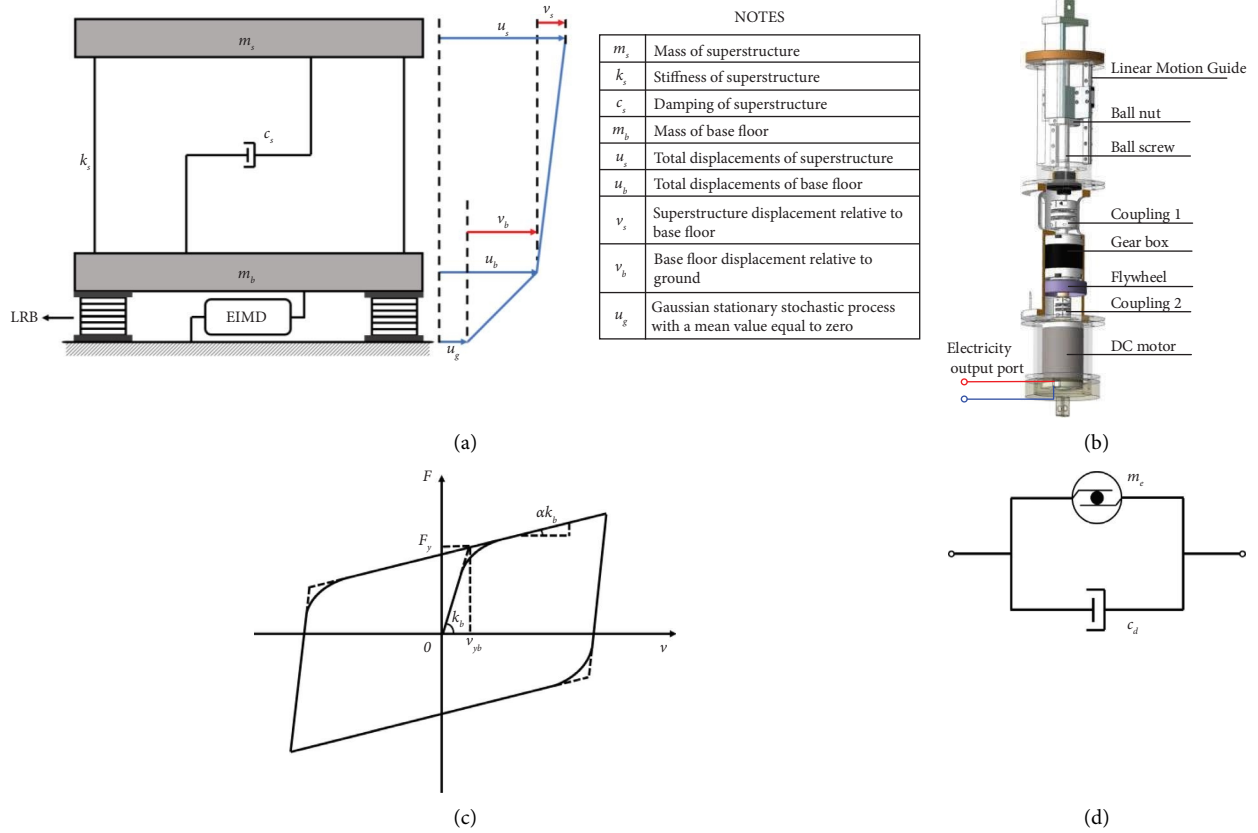


FIGURE 1: Configuration of the EIMD and the 2-DOF model of a structure with the hybrid base isolation system. (a) Configuration of the hybrid base isolation system; (b) configuration of the EIMD; (c) Bouc-Wen hysteretic model of LRB; (d) mechanical model of EIMD.

Substituting equations (1), (2), and (3) into equation (4), we have

$$m_s \ddot{v}_s + m_s \ddot{v}_b + c_s \dot{v}_s + k_s v_s = -m_s \ddot{u}_g, \quad (5a)$$

$$m_s \ddot{v}_s + (m_s + m_b + m_e) \ddot{v}_b + (c_b + c_d) \dot{v}_b + \alpha k_b v_b + (1 - \alpha) k_b v_{yb} Z = -(m_s + m_b) \ddot{u}_g, \quad (5b)$$

$$v_{yb} \dot{Z} = A \dot{v}_b - \gamma |\dot{v}_b| |Z|^{\eta-1} Z - \beta \dot{v}_b |Z|^\eta. \quad (5c)$$

2.2. Stationary Stochastic Seismic Excitation Model. The stationary stochastic seismic excitation model can be adopted as the Kanai-Tajimi filtered Gaussian white-noise process, which is given by the following differential equations::

$$u_g = -2\xi_f \omega_f \dot{u}_{f_2} - \omega_f^2 u_{f_2} + 2\xi_g \omega_g \dot{u}_{f_1} + \omega_g^2 u_{f_1}, \quad (6a)$$

$$\ddot{u}_{f_2} + 2\xi_f \omega_f \dot{u}_{f_2} + \omega_f^2 u_{f_2} = -(\ddot{u}_{f_1} + w), \quad (6b)$$

$$\ddot{u}_{f_1} + 2\xi_g \omega_g \dot{u}_{f_1} + \omega_g^2 u_{f_1} = -w, \quad (6c)$$

where w is the Gaussian white-noise process with a mean value equal to zero at the bedrock. u_{f_1} , ω_g , and ξ_g are the displacement response, natural frequency, and damping

ratio of the first filter, respectively. u_{f_2} , ω_f , and ξ_f are the displacement response, natural frequency, and damping ratio of the second filter, respectively. The two-sided power spectrum density (PSD) function of the Kanai-Tajimi filtered Gaussian white-noise process is given by

$$S_{\ddot{u}_g} = \frac{\omega_g^4 + 4\xi_g^2 \omega_g^2 \omega^2}{(\omega_g^2 - \omega^2)^2 + 4\xi_g^2 \omega_g^2 \omega^2} \frac{\omega^4}{(\omega_f^2 - \omega^2)^2 + 4\xi_f^2 \omega_f^2 \omega^2} S_0, \quad (7)$$

where S_0 is the bedrock white-noise input intensity, which can be calculated by

$$S_0 = \frac{0.141 \xi_g \ddot{u}_{g,\max}^2}{\omega_g \sqrt{1 + 4\xi_g^2}}, \quad (8)$$

and the $\ddot{u}_{g,\max}$ is the peak ground acceleration (PGA). $\ddot{u}_{g,\max}$ is taken as 0.4 g in the study.

2.3. Statistical Linearization Technique. The statistical linearization technique is adopted to deal with the nonlinear equation in equation (5). Equation (5c) can be replaced by the following equivalent linear equation:

$$v_{yb} \dot{Z} + c_{eq} \dot{v}_b + k_{eq} Z = 0, \quad (9)$$

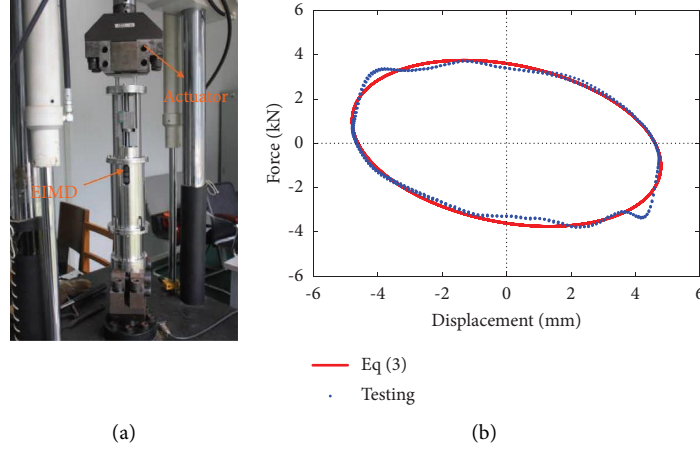


FIGURE 2: Validation of the EIMD model (parameters of the EIMD prototype: $m_e = 5.8$ ton, $c_d = 132.4 \text{ kN} \cdot \text{s}/\text{m}$, and $R_{\text{load}} = 0 \Omega$; sinusoidal excitation frequency: 1 Hz, displacement amplitude: 5 mm). (a) Experimental setup; (b) comparison of predicted and measured hysteretic curve of the EIMD.

where c_{eq} and k_{eq} are the equivalent linear damping and stiffness coefficients of the LRB, respectively. The linearization coefficients c_{eq} and k_{eq} can be computed by minimizing the expectation of the least square error between the nonlinear equation (5c) and linearized equation (9), which are given by

$$c_{eq} = \sqrt{\frac{2}{\pi}} \left\{ \gamma \frac{E[\dot{v}_b Z]}{\sigma_{\dot{v}_b}} + \beta \sigma_Z \right\} - A, \quad (10a)$$

$$k_{eq} = \sqrt{\frac{2}{\pi}} \left\{ \gamma \sigma_{\dot{v}_b} + \beta \frac{E[\dot{v}_b Z]}{\sigma_Z} \right\}, \quad (10b)$$

where $E[\bullet]$ denotes the expectation operator.

2.4. State-Space Model of the BIS. A state-space model is adopted to solve the response of the equivalent linear system. Equations (5a) and (5b) can be rewritten as

$$\begin{bmatrix} m_s + m_b + m_e & m_s \\ m_s & m_s \end{bmatrix} \begin{bmatrix} \ddot{v}_b \\ \ddot{v}_s \end{bmatrix} + \begin{bmatrix} c_b + c_d & 0 \\ 0 & c_s \end{bmatrix} \begin{bmatrix} \dot{v}_b \\ \dot{v}_s \end{bmatrix} + \begin{bmatrix} \alpha k_b & 0 \\ 0 & k_s \end{bmatrix} \begin{bmatrix} v_b \\ v_s \end{bmatrix} + \begin{bmatrix} (1-\alpha)k_b v_{yb} \\ 0 \end{bmatrix} Z = \begin{bmatrix} -(m_s + m_b)\ddot{u}_g \\ -m_s \ddot{u}_g \end{bmatrix}. \quad (11)$$

Write equation (11) in standard form as

$$\mathbf{M}\ddot{\mathbf{v}} + \mathbf{C}\dot{\mathbf{v}} + \mathbf{K}\mathbf{v} + \mathbf{H}Z = -\mathbf{I}\ddot{u}_g, \quad (12)$$

where

$$\mathbf{M} = \begin{bmatrix} 1 + \mu & \gamma \\ 1 & 1 \end{bmatrix}, \mathbf{C} = \begin{bmatrix} 2\xi_b \omega_b + 2\xi \omega_b & 0 \\ 0 & 2\xi_s \omega_s \end{bmatrix}, \mathbf{K} = \begin{bmatrix} \omega_b^2 & 0 \\ 0 & \omega_s^2 \end{bmatrix}, \mathbf{H} = \begin{bmatrix} (1-\alpha)\omega_b^2 v_{yb} \\ \alpha \\ 0 \end{bmatrix}, \mathbf{v} = \begin{bmatrix} v_b \\ v_s \end{bmatrix}, \mathbf{I} = \begin{bmatrix} 1 \\ 1 \end{bmatrix}, \quad (13)$$

in which the natural frequency and damping ratio of the BIS and the superstructure are as follows: $\omega_b = \sqrt{\alpha k_b / (m_s + m_b)}$ and

$\xi_b = c_b / [2(m_s + m_b)\omega_b]$; $\omega_s = \sqrt{k_s / m_s}$ and $\xi_s = c_s / 2m_s \omega_s$, respectively; $\gamma = m_s / (m_s + m_b)$ represents the mass ratio of the

BIS; $\mu = m_e/(m_s + m_b)$ and $\xi = c_d/[2(m_s + m_b)\omega_b]$ represent the inertance-to-mass ratio and the damping ratio of the EIMD, respectively.

Equations (9) and (11) can be written in the state-space form as

$$\dot{\mathbf{V}} = \mathbf{B}\mathbf{V} + \mathbf{W}, \quad (14)$$

$$\mathbf{B} = \begin{bmatrix} \mathbf{0}_{2 \times 2} & \mathbf{E}_{2 \times 2} & \mathbf{0}_{2 \times 1} & \mathbf{0}_{2 \times 1} & \mathbf{0}_{2 \times 1} & \mathbf{0}_{2 \times 1} & \mathbf{0}_{2 \times 1} \\ -\mathbf{M}^{-1}\mathbf{K} & -\mathbf{M}^{-1}\mathbf{C} & -\mathbf{M}^{-1}\mathbf{H} & \mathbf{M}^{-1}\mathbf{I}\omega_f^2 & \mathbf{M}^{-1}\mathbf{I}2\xi_f\omega_f & -\mathbf{M}^{-1}\mathbf{I}\omega_g^2 & -\mathbf{M}^{-1}\mathbf{I}2\xi_g\omega_g \\ \mathbf{0}_{1 \times 2} & \left\{ \begin{array}{c} c_{eq} \\ v_{yb} \end{array} \right\} & \frac{k_{eq}}{v_{yb}} & 0 & 0 & 0 & 0 \\ \mathbf{0}_{1 \times 2} & \mathbf{0}_{1 \times 2} & 0 & 0 & 1 & 0 & 0 \\ \mathbf{0}_{1 \times 2} & \mathbf{0}_{1 \times 2} & 0 & -\omega_f^2 & -2\xi_f\omega_f & \omega_g^2 & 2\xi_g\omega_g \\ \mathbf{0}_{1 \times 2} & \mathbf{0}_{1 \times 2} & 0 & 0 & 0 & 0 & 1 \\ \mathbf{0}_{1 \times 2} & \mathbf{0}_{1 \times 2} & 0 & 0 & 0 & -\omega_g^2 & -2\xi_g\omega_g \end{bmatrix}, \quad (16)$$

and \mathbf{W} is the excitation vector, that is,

$$\mathbf{W} = \{0, 0, 0, 0, 0, 0, 0, -\omega\}^T. \quad (17)$$

The state vector \mathbf{V} is a Markov process, and the Γ is the covariance matrix of the response vector \mathbf{V} and satisfies the following equation:

$$\dot{\Gamma} = \mathbf{B}\Gamma + \Gamma\mathbf{B}^T + \mathbf{D}, \quad (18)$$

where \mathbf{D} represents the input matrix of the bedrock excitation, which is given by

$$\mathbf{D} = \begin{bmatrix} \mathbf{0}_{8 \times 8} & \mathbf{0}_{8 \times 1} \\ \mathbf{0}_{1 \times 8} & 2\pi S_0 \end{bmatrix}. \quad (19)$$

The elements of the response covariance matrix Γ read

$$\Gamma_{ij} = \mathbf{E}(\mathbf{V}_i \mathbf{V}_j). \quad (20)$$

In the steady-state, the matrix Γ is independent of time, then $\dot{\Gamma}$ equal to zeros. Equation (18) becomes a reduced Lyapunov equation as

$$\mathbf{B}\Gamma + \Gamma\mathbf{B}^T + \mathbf{D} = \mathbf{0}. \quad (21)$$

Equation (21) can be solved using MATLAB directly. The linearization coefficients c_{eq} and k_{eq} are initially unknown.

where the state vector \mathbf{V} is defined as

$$\mathbf{V} = \{v_b, v_s, \dot{v}_b, \dot{v}_s, Z, u_{f_2}, \dot{u}_{f_2}, u_{f_1}, \dot{u}_{f_1}\}^T, \quad (15)$$

and \mathbf{B} is the augmented system matrix, which is given by

Given the appropriate initial values of the c_{eq} and k_{eq} and establishing the matrix \mathbf{B} the updated c_{eq} and k_{eq} can be obtained by solving Equation (21), and then by conducting an iterative calculation, the c_{eq} and k_{eq} can be determined upon reaching convergence.

3. Parametric Optimization

3.1. Effect of EIMD Parameters on Seismic Response Control. A parametric analysis is conducted to investigate the effect of EIMD parameters on seismic response control for the BIS. We define three performance indicators using the response variances of the superstructure relative displacement ($\sigma_{v_s}^2$), the superstructure absolute acceleration ($\sigma_{\ddot{u}_s}^2$), and the base floor relative displacement ($\sigma_{v_b}^2$). The $\sigma_{v_s}^2$ and $\sigma_{v_b}^2$ can be directly obtained from the response variances matrix Γ . We know the absolute acceleration \ddot{u}_s satisfies the following equation, that is,

$$\ddot{u}_s = \ddot{v}_b + \ddot{v}_s + \ddot{u}_g, \quad (22)$$

and through equation (4a), the following equation can be obtained:

$$\ddot{u}_s = -2\xi_s\omega_s\dot{v}_s - \omega_s^2v_s. \quad (23)$$

Then, the $\sigma_{\dot{u}_s}^2$ can be given by

$$\sigma_{\dot{u}_s}^2 = E\left[\dot{u}_s^2\right] = 4\xi_s^2\omega_s^2\sigma_{v_s}^2 + \omega_s^4\sigma_{v_s}^2. \quad (24)$$

The parameters of the 2-DOF dynamical model of the BIS with the hybrid base isolation system are set as follows:

$$\text{superstructure: } m_s = 21015 \text{ tons, } k_s = 1195770 \frac{\text{kN}}{\text{m}}, \xi_s = 0.02, \quad (25a)$$

$$\text{base floor: } m_b = 6115 \text{ tons,} \quad (25b)$$

$$\text{LRB: } k_b = 1713679 \frac{\text{kN}}{\text{m}}, \xi_b = 0.05, \alpha = 0.1, \quad (25c)$$

$$\cdot v_{yb} = 0.015 \text{ m, } A = 1, \beta = \gamma = 0.5, \eta = 1.$$

The fundamental periods of the superstructure and the BIS are

$$T_s = \frac{2\pi}{\omega_s} = \frac{2\pi}{\sqrt{k_s/m_s}} = 0.83\text{s}, T_b = \frac{2\pi}{\omega_b} = \frac{2\pi}{\sqrt{\alpha k_b/(m_b + m_s)}} = 2.5\text{s}. \quad (26)$$

The parameters of the Kanai-Tajimi filtered Gaussian white-noise process are $\omega_g = 15.0 \text{ rad/s}$, $\xi_g = 0.6$, $\omega_f = 1.5$, and $\xi_f = 0.6$ (for the firm soil condition) and $\omega_g = 5.0 \text{ rad/s}$, $\xi_g = 0.2$, $\omega_f = 0.5$, and $\xi_f = 0.6$ (for the soft soil condition).

Figures 3(a)–3(c) show the seismic response reduction ratio of the BIS under firm soil conditions varying with the parameters of the EIMD. The $\sigma_{v_{b0}}^2$, $\sigma_{v_{s0}}^2$, and $\sigma_{\dot{u}_{s0}}^2$ are the responses of the BIS without dampers. In the study, the inertance-to-mass ratio μ and the damping ratio coefficient ξ of the EIMD are limited to a reasonable range: $0 \leq \mu \leq 1$ and $0 \leq \xi \leq 0.5$. It is observed in Figure 3(a) that the variation of the damping ratio ξ has a greater effect on reducing the base floor displacement response variance than that of the inertance-to-mass ratio μ . From Figures 3(b) and 3(c), it is found that there are an optimal inertance and damping for minimizing the relative displacement or absolute acceleration response of the superstructure. A similar change rule of the seismic responses versus the parameters of the EIMD can also be obtained in the soft soil condition, as shown in Figure 4. In addition, compared with Figures 3 and 4, we found that the EIMD is more effective in soft soil conditions than in firm soil conditions.

3.2. Optimization Procedure. The previous analysis verifies the effectiveness of the EIMD in reducing the seismic response of the BIS. Results illustrate that there is an optimal inertance-to-mass ratio μ and damping ratio ξ to minimize the response variance of the superstructure (relative displacement or absolute acceleration). This section proposes a stochastic optimization procedure of the EIMD to minimize the relative displacement response variance of the

superstructure. It can be transformed into a constrained optimization problem as follows:

$$\min_{\mathbf{x}} \sigma_{v_s}^2 \text{ such that } \mathbf{x}_{lb} \leq \mathbf{x} \leq \mathbf{x}_{ub}, \quad (27)$$

where $\mathbf{x} = [\mu, \xi]$ represents the parameter vector of the EIMD; \mathbf{x}_{lb} and \mathbf{x}_{ub} are the lower and upper values of \mathbf{x} . We solve equation (27) by using a nonlinear programming solver (fmincon function) in MATLAB®.

The following optimization procedure is depicted in Figure 5:

- (1) Based on the 2-DOF base-isolated model, we establish the relationship between the response variance $\sigma_{v_s}^2$ and the parameters (μ, ξ) through equations (20) and (21).
- (2) We solve equation (27) and obtain the optimal parameters μ, ξ .

3.3. Parametric Study. Based on the above stochastic optimization procedure, we study optimal parameters and corresponding seismic response control effects of the EIMD considering different α of the LRB under firm and soft soil conditions. Considering the same system parameters as shown in equation (25), the value of α ranges from 0.05 up to 0.15, corresponding to the isolation period $T_b = 3.54\text{s}$ to $T_b = 2.04\text{s}$, respectively. From Figure 6, we can find the following:

- (1) It can be seen from Figure 6(a) that, in the two soil conditions, with the increase of α , that is, the decrease of the isolation period T_b , the optimal inertance-to-mass ratio μ also increases. This means that the lower the isolation period of the system, the greater the inertance of the EIMD is needed. Under soft soil conditions, the optimal μ becomes larger compared with the cases of firm soil conditions.
- (2) As shown in Figure 6(b), the optimal damping coefficient ξ is positively correlated with α , and the optimal ξ is larger in soft soil conditions than in firm soil conditions.
- (3) Figure 6(c) shows the reduction ratio of the relative displacement response variance $\sigma_{v_s}^2$ of the LRB-isolated structure with optimal EIMD. When α increases from 0.05 to 0.15, the reduction ratio of $\sigma_{v_s}^2$ in the case of firm soil conditions ranges from 17.4% to 30.6%, whereas in the soft soil condition case, it ranges from 34.4% up to 71.8%. It is observed that the EIMD performs better for controlling the superstructure relative displacement response variance in soft soil conditions.

4. Numerical Simulation

A seven-story LRB-isolated building [23] is selected as the numerical model in this numerical simulation study, as shown in Figure 7. The building is located at a soft soil site.

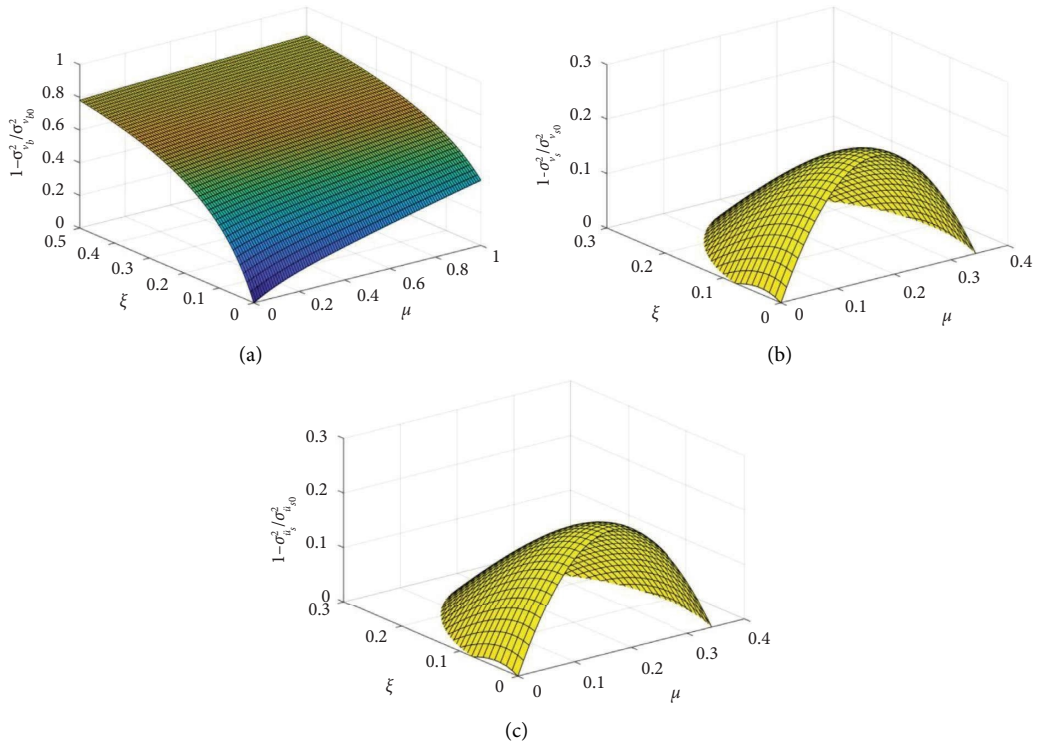


FIGURE 3: Relationship between the reduction ratios of system response variances and the EIMD parameters under firm soil conditions. (a) Reduction ratio of $\sigma_{v_b}^2$ versus μ and ξ . (b) Reduction ratio of $\sigma_{v_s}^2$ versus μ and ξ . (c) Reduction ratio of $\sigma_{u_s}^2$ versus μ and ξ .

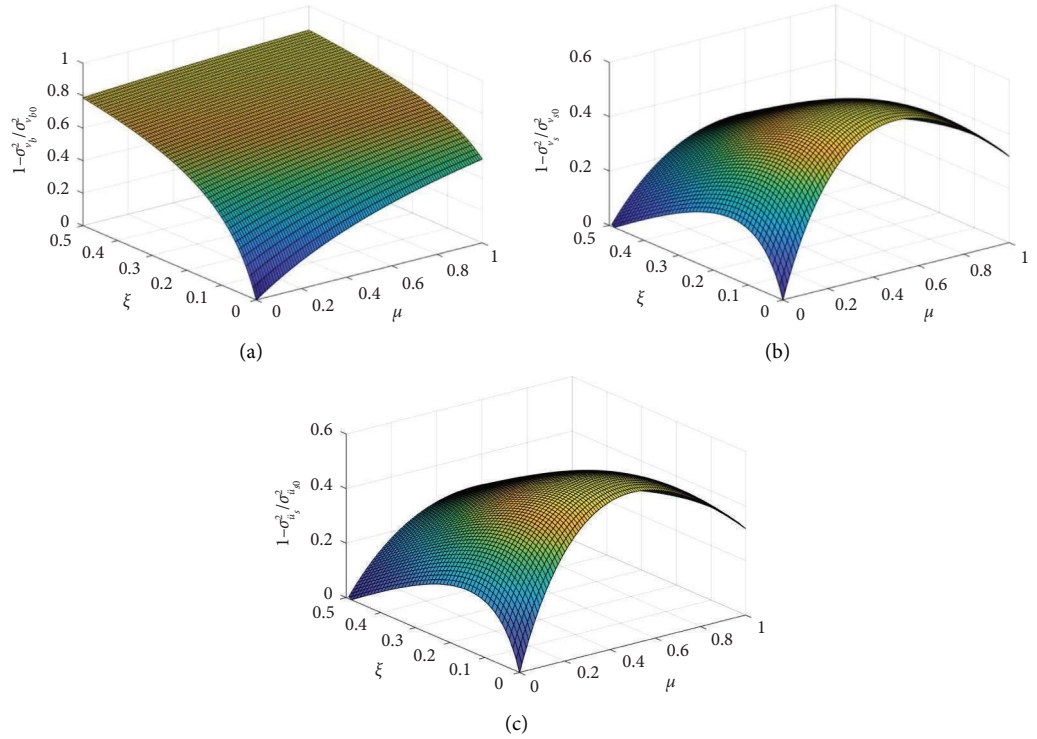


FIGURE 4: Relationship between the reduction ratios of system response variances and the EIMD parameters under soft soil conditions. (a) Reduction ratio of $\sigma_{v_b}^2$ versus μ and ξ . (b) Reduction ratio of $\sigma_{v_s}^2$ versus μ and ξ . (c) Reduction ratio of $\sigma_{u_s}^2$ versus μ and ξ .

The superstructure is assumed to remain in a linear state when experiencing earthquakes. A bilinear model with viscous damping is used to describe the hysteretic behavior of the LRB, of which the parameters are $\xi_b = 0.05$, $\alpha = 0.1$, $v_{yb} = 0.015$ m, $A = 1$, $\beta = \gamma = 0.5$, and $\eta = 1$. Thus, the isolation period of the LRB-isolated building is $T_b = 2.5$ s. In this numerical simulation, the nonlinear time-history responses are obtained using the Runge-Kutta method with a fixed step of 0.001 s.

4.1. Design of a EIMD. Based on a 2-DOF analytical model, the optimal EIMD parameters can be obtained using the proposed stochastic optimization procedure. Figure 7 shows the specifications of the equivalent 2-DOF model of the seven-story LRB-isolated building. In the parameter optimization, the bound of \mathbf{x} is given by

$$\mathbf{x}_{lb} = [0; 0], \mathbf{x}_{ub} = [1; 0.5]. \quad (28)$$

Solving equation (27), the optimal parameters of the EIMD are $\mu = 0.47$ and $\xi = 0.06$.

Except for the hybrid base isolation system with the EIMD, the case of the viscous damper (VD) is also computed for comparison purposes. Using the same optimization procedure (let $m_e = 0$), the optimal damping ratio of VD is 0.15.

4.2. Nonlinear Seismic Response Analysis. This section presents the nonlinear seismic response analysis of the building model with the hybrid base isolation system. The differential equations of motion of the system are as follows:

$$\mathbf{M}^* \mathbf{v} + \mathbf{C}^* \dot{\mathbf{v}} + \mathbf{K}^* \mathbf{v} + \mathbf{H}^* Z = -\bar{\mathbf{M}}^* u_g, \quad (29a)$$

$$v_{yb} \dot{Z} = A \dot{v}_b - \gamma |\dot{v}_b| |Z|^{\eta-1} Z - \beta \dot{v}_b |Z|^\eta, \quad (29b)$$

in which

$$\mathbf{M}^* = \begin{bmatrix} \left(m_b + \sum_{i=1}^7 m_i \right) + m_e & m_1 & m_2 & m_3 & m_4 & m_5 & m_6 & m_7 \\ m_1 & m_1 & 0 & 0 & 0 & 0 & 0 & 0 \\ m_2 & 0 & m_2 & 0 & 0 & 0 & 0 & 0 \\ m_3 & 0 & 0 & m_3 & 0 & 0 & 0 & 0 \\ m_4 & 0 & 0 & 0 & m_4 & 0 & 0 & 0 \\ m_5 & 0 & 0 & 0 & 0 & m_5 & 0 & 0 \\ m_6 & 0 & 0 & 0 & 0 & 0 & m_6 & 0 \\ m_7 & 0 & 0 & 0 & 0 & 0 & 0 & m_7 \end{bmatrix}, \quad (30a)$$

$$\mathbf{C}^* = \begin{bmatrix} c_b + c_d & 0 & 0 & 0 & 0 & 0 & 0 & 0 \\ 0 & c_1 + c_2 & -c_2 & 0 & 0 & 0 & 0 & 0 \\ 0 & -c_2 & c_2 + c_3 & -c_3 & 0 & 0 & 0 & 0 \\ 0 & 0 & -c_3 & c_3 + c_4 & -c_4 & 0 & 0 & 0 \\ 0 & 0 & 0 & -c_4 & c_4 + c_5 & -c_5 & 0 & 0 \\ 0 & 0 & 0 & 0 & -c_5 & c_5 + c_6 & -c_6 & 0 \\ 0 & 0 & 0 & 0 & 0 & -c_6 & c_6 + c_7 & -c_7 \\ 0 & 0 & 0 & 0 & 0 & 0 & -c_7 & c_7 \end{bmatrix}, \quad (30b)$$

$$\mathbf{K}^* = \begin{bmatrix} \alpha k_b & 0 & 0 & 0 & 0 & 0 & 0 & 0 \\ 0 & k_1 + k_2 & -k_2 & 0 & 0 & 0 & 0 & 0 \\ 0 & -k_2 & k_2 + k_3 & -k_3 & 0 & 0 & 0 & 0 \\ 0 & 0 & -k_3 & k_3 + k_4 & -k_4 & 0 & 0 & 0 \\ 0 & 0 & 0 & -k_4 & k_4 + k_5 & -k_5 & 0 & 0 \\ 0 & 0 & 0 & 0 & -k_5 & k_5 + k_6 & -k_6 & 0 \\ 0 & 0 & 0 & 0 & 0 & -k_6 & k_6 + k_7 & -k_7 \\ 0 & 0 & 0 & 0 & 0 & 0 & -k_7 & k_7 \end{bmatrix}, \quad (30c)$$

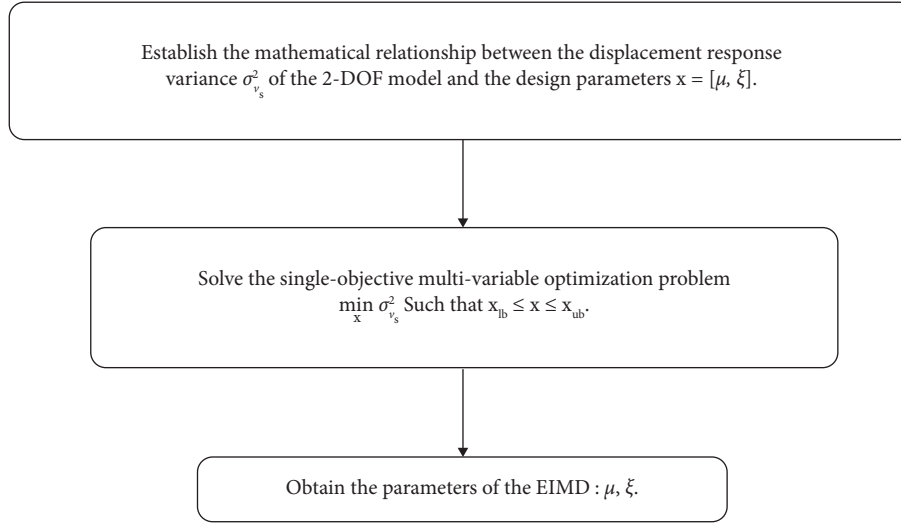


FIGURE 5: Flowchart of the design of the EIMD.

$$\mathbf{H}^* = \begin{bmatrix} (1 - \alpha)k_b v_{yb} \\ 0 \\ 0 \\ 0 \\ 0 \\ 0 \\ 0 \\ 0 \end{bmatrix}, \bar{\mathbf{M}}^* = \left[m_b + \sum_{i=1}^7 m_i m_1 m_2 m_3 m_4 m_5 m_6 m_7 \right], \mathbf{v} = \begin{bmatrix} v_b \\ v_1 \\ v_2 \\ v_3 \\ v_4 \\ v_5 \\ v_6 \\ v_7 \end{bmatrix}. \quad (30d)$$

The natural periods of the fix-base building model are 0.833 s, 0.294 s, 0.193 s, 0.148 s, 0.128 s, 0.110 s, and 0.093 s, respectively. The LRB's elastic stiffness k_b can be calculated by the following formula:

$$k_b = \frac{(m_b + \sum_{i=1}^7 m_i) \cdot (2\pi/T_b)^2}{\alpha} = 1912019 \frac{kN}{m}. \quad (31)$$

Then, the isolation period of the LRB-isolated building is 2.60 s.

According to Section 4.1, the optimal parameters of the EIMDs are $m_e = 14226.9\text{ton}$ and $c_d = 9129.2 \text{ kN} \cdot \text{s}/m$, respectively.

4.2.1. Results of Artificial Excitations. Based on the filtered Kanai-Tajimi spectrum (in equation (7)) and the parameters of soft soil conditions, 100 stationary artificial accelerograms are generated using the spectral representation method [32]. We take the data point number of every single artificial accelerogram as 8192 data points to ensure higher computational efficiency in the fast Fourier transform (FFT). The time interval is 0.02 s, so the duration of each artificial accelerogram is 163.84 s. A time-modulating function is used to multiply the 100 stationary artificial accelerograms

to obtain the nonstationary artificial accelerograms, which are given by [33]

$$g(t) = a_1 t \exp(-a_2 t), \quad (32)$$

where $a_1 = 0.45\text{s}^{-1}$ and $a_2 = 1/6\text{s}^{-1}$.

A typical nonstationary artificial accelerogram with a peak acceleration equal to 0.4 g is plotted in Figure 8. Figures 9(a) and 9(b) show the hysteretic behaviors of the two dampers under the artificial seismic excitations, respectively. The maximum damper force of the VD is 32760 kN, while the counterpart of the EIMD is 66699 kN, which is about twice that of the former. In addition, it is also observed that the hysteretic behaviors of the EIMD have an obvious negative slope in the second and fourth quadrants, which partially simulates the characteristics of active control force.

Figure 10 compares the seismic time-history responses of the BIS model subjected to the artificial seismic excitations in three cases: without damper, with the VD, and with the EIMD. It can be seen from Figures 10(a)–10(c) that the EIMD performs much better than the VD. On the one hand, in the LRB-isolated structure with the EIMD, the maximum values of the base floor deformation, superstructure inter-story drift, and superstructure acceleration are reduced by

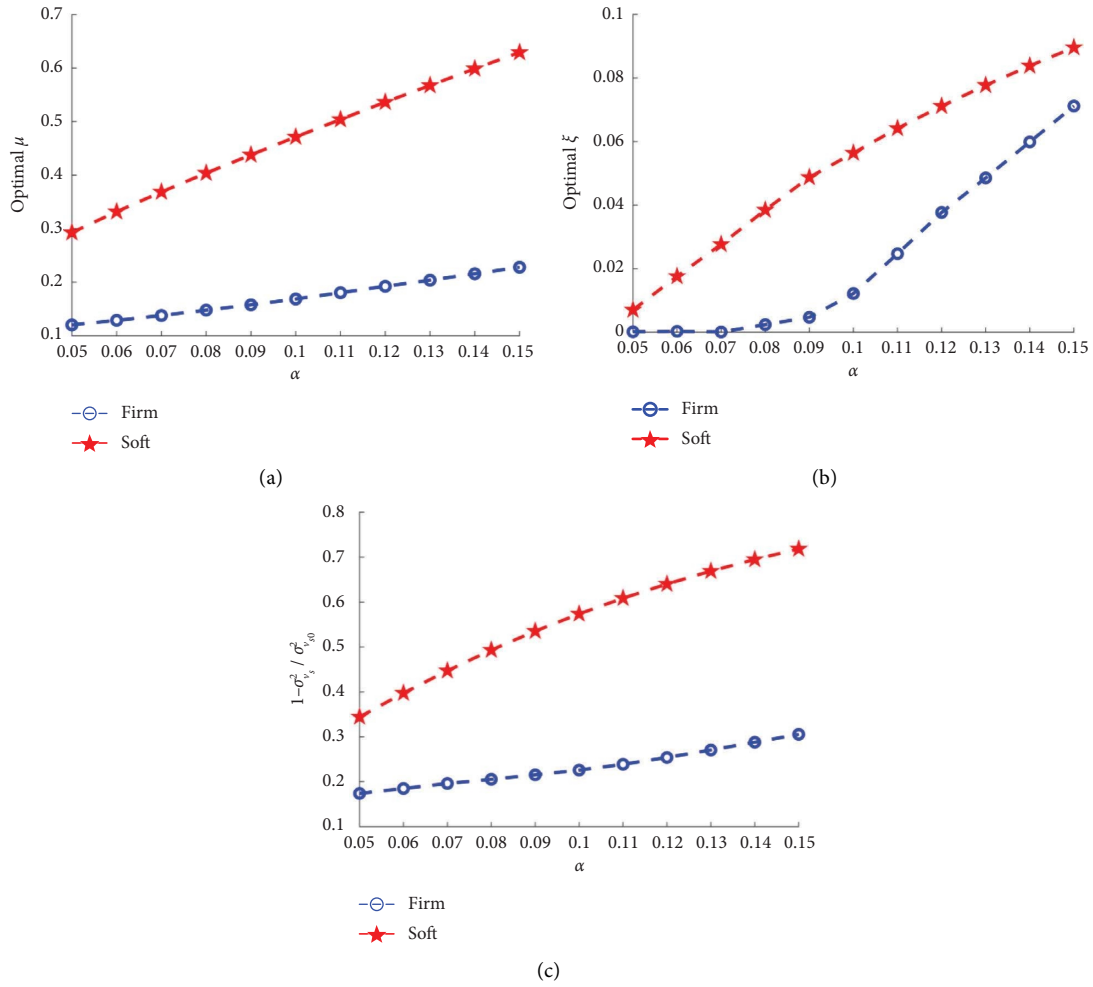


FIGURE 6: Effect of α on optimal μ , ξ , and response reduction ratio. (a) Inertance-to-mass ratio μ . (b) Damping ratio coefficient ξ . (c) Reduction ratio of $\sigma_{v_y}^2$.

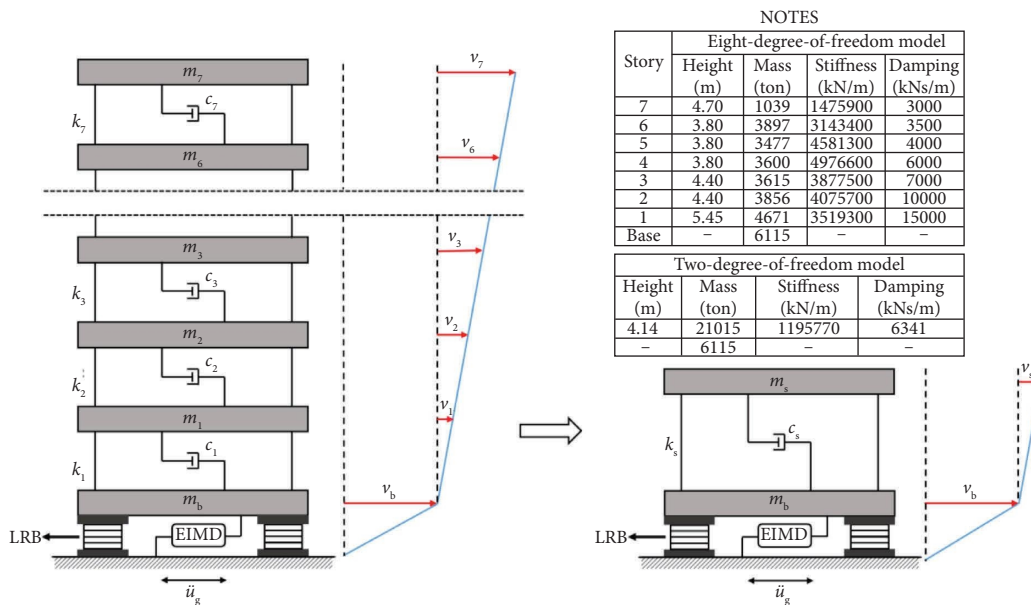


FIGURE 7: The seven-story base-isolated building with an EIMD.

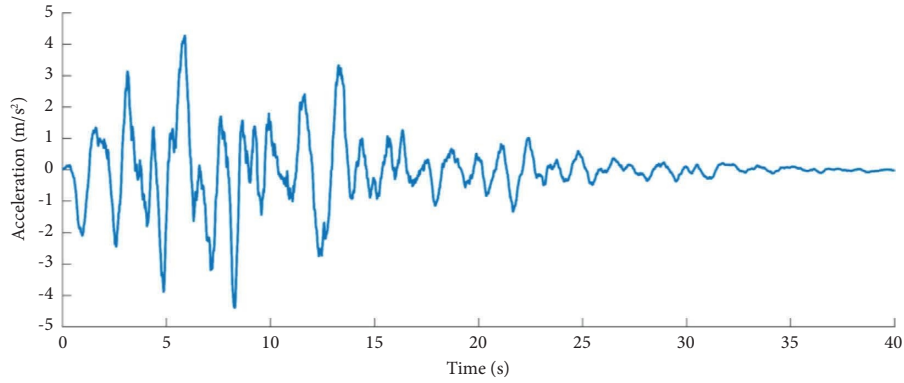


FIGURE 8: Typical artificial accelerograms (soft soil condition, $\ddot{u}_{g,max} = 0.4g$).

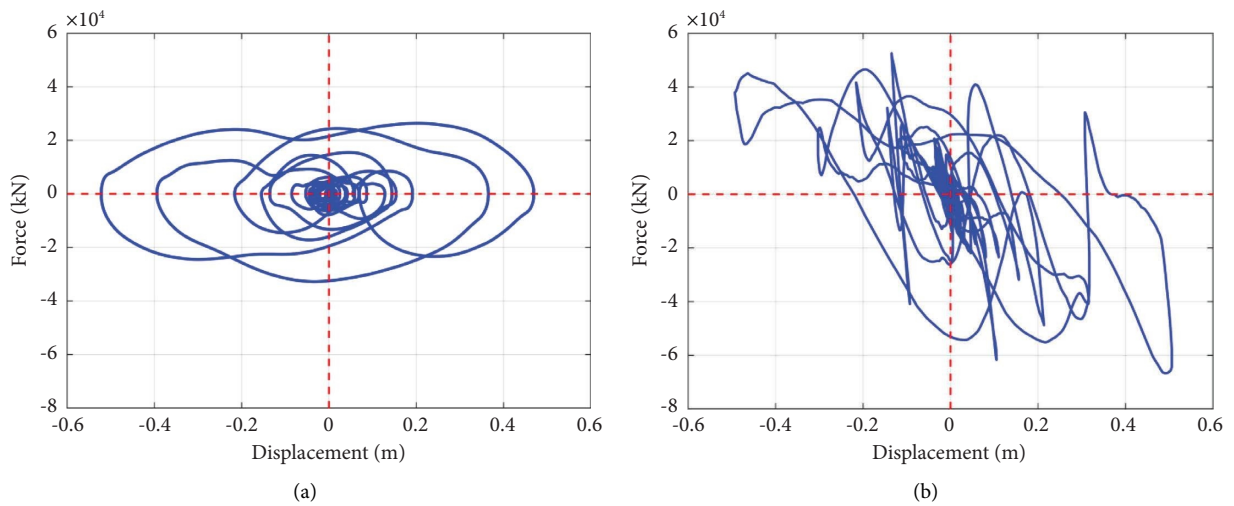


FIGURE 9: Typical force-displacement curves of VD and EIMD under artificial seismic excitations. (a) VD. (b) EIMD.

37.2%, 50.3%, and 40.3%, respectively, whereas in the VD case, they are reduced by 35.3%, 30.2%, and 26.3%, respectively.

Figure 11 plots the average peak displacement response of the analytical model under 100 artificial excitations in the three cases: without damper, with the VD, and with the EIMD. It can be seen that the EIMD reduces the interstory drifts more effectively than the VD. The peak absolute acceleration occurs on the roof, whereas the peak interstory drift takes place on the first floor. Detailed information on the average peak seismic responses of the three cases is shown in Figure 12. When the LRB-isolated structure is coupled with the EIMD, the interstory drift of the 1st floor is decreased from 0.0314 m to 0.0221 m, the relative displacement of the base floor is decreased from 0.5359 m to 0.3929 m, and the absolute acceleration of the roof is decreased from 8.0905 m/s² to 5.2827 m/s², respectively. In summary, numerical results illustrate that the EIMD outperforms the VD.

4.2.2. Results of Earthquake Records. According to Eurocode 8, [34] a set of real ground motion records (soft soil

condition, $V_{s30} < 180$ m/s) is used to conduct a nonlinear seismic response analysis of the building model with different dampers. Table 1 lists detailed information about the ground motion records. For consistency with the numerical simulation of artificial seismic excitation cases, the PGA of the ground motion records was scaled to 0.4 g. Figure 13 plots the accelerograms of the Chuetsu-oki earthquake (RSN-5295). Figure 14 compares the normalized PSD of the ground motion record with the normalized Kanai-Tajimi spectrum (in equation (7)). It is found that their frequency components are fairly matched.

Figure 15 compares the time-history responses of the analytical model subjected to the Chuetsu-oki earthquake (RSN-5295) in three cases: without damper, with the VD, and with the EIMD. When the LRB-isolated structure is coupled with the EIMD, the maximum values of base floor deformation, superstructure interstory drift, and superstructure acceleration are reduced by 29.7%, 34.5%, and 42.5%, respectively. The corresponding results are 26.3%, 17.1%, and 4.4%, respectively, for the LRB-isolated structure with the VD. As a result, the EIMD outperforms the VD in reducing the seismic response of the LRB-isolated structure under the Chuetsu-oki earthquake (RSN-5295).

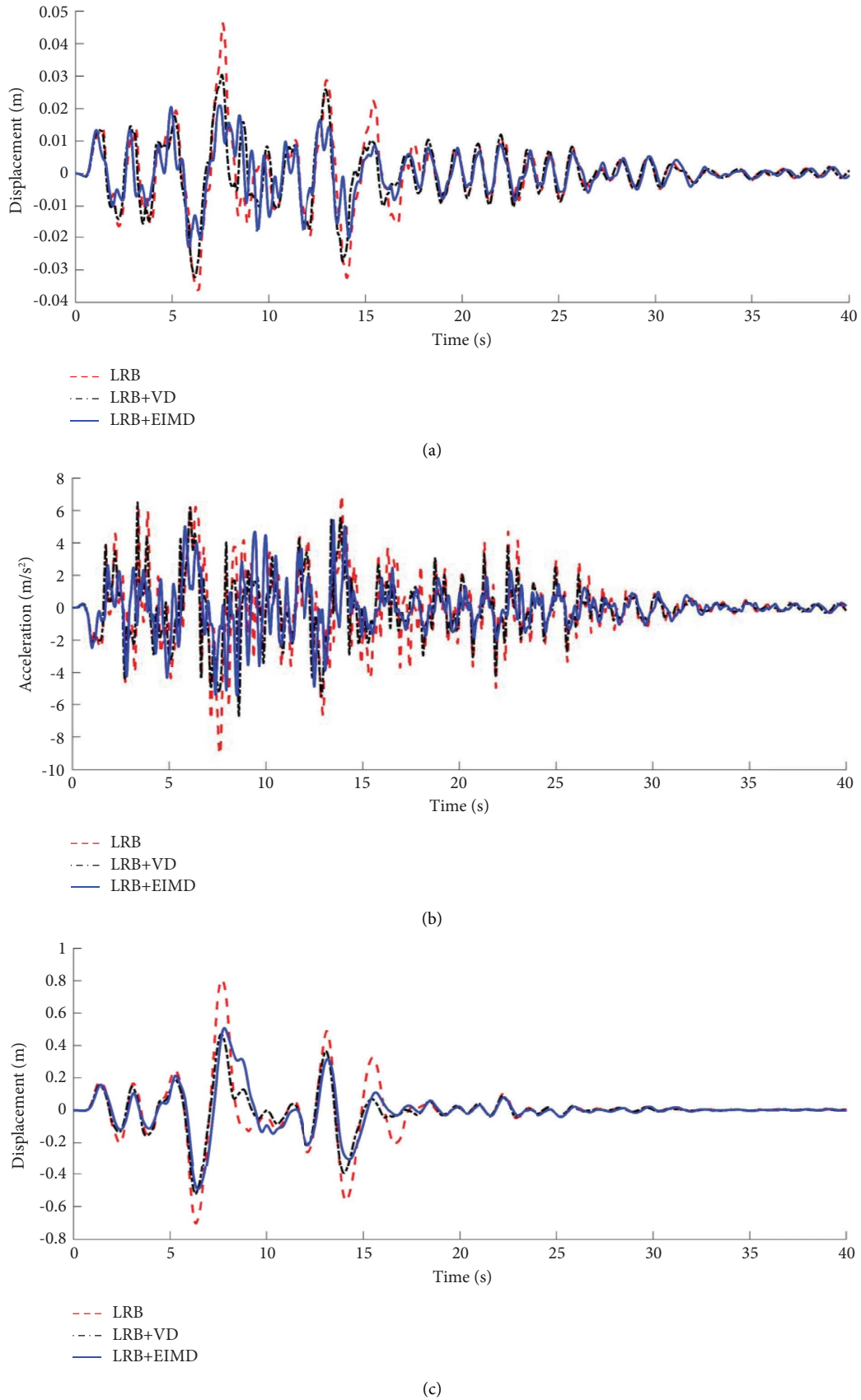


FIGURE 10: Comparison of the seismic responses of the three cases subjected to the artificial accelerogram (soft soil condition, $PGA = 0.4 g$). (a) Interstory drift at the first floor of the superstructure. (b) Absolute acceleration at the roof. (c) Base floor deformation.

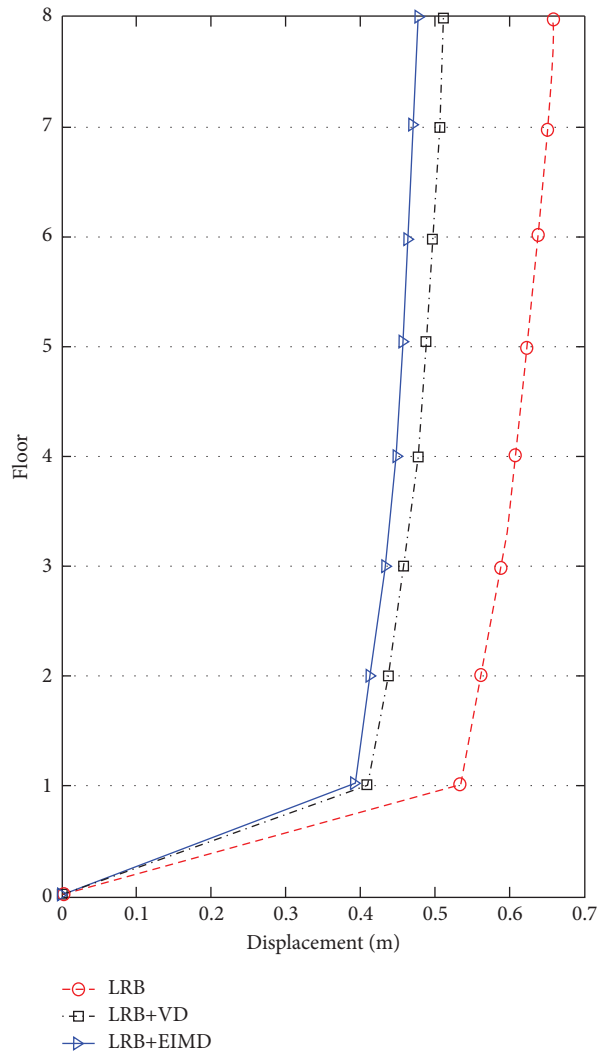


FIGURE 11: Average peak displacement responses of the seven-story LRB-isolated building with or without dampers subjected to a total of 100 artificial accelerograms (soft soil condition, PGA = 0.4 g).

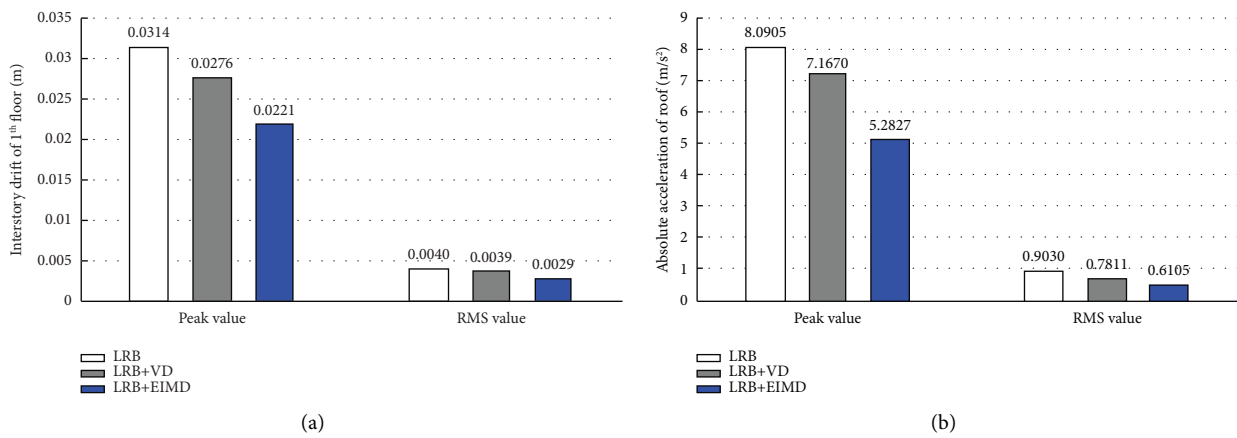
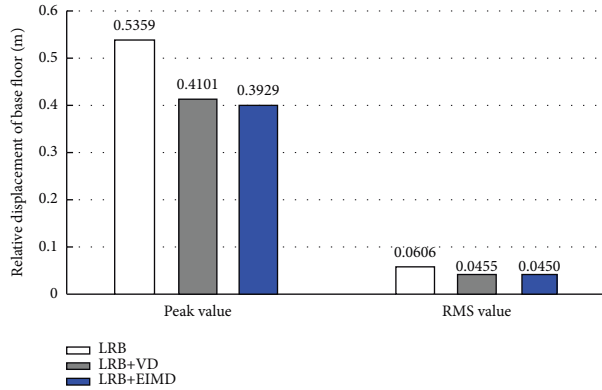


FIGURE 12: Continued.



(c)

FIGURE 12: Comparison of the control performances of the EIMD and VD for the seven-story LRB-isolated building subjected to a total of 100 artificial seismic excitations (PGA = 0.4 g). (a) Interstory drift at the first floor of the superstructure. (b) Absolute acceleration at the roof. (c) Base floor deformation.

TABLE 1: Information of the ground motion records.

Record sequence	Event	Year	Station	Magnitude	Rupture distance (km)	V_{s30} (m/s)	Component
5295	Chuetsu-oki, Japan	2007	SIT003	6.8	169.99	99.93	NS
6443	Niigata, Japan	2004	AIC003	6.63	292.12	144.37	EW
4941	Chuetsu-oki, Japan	2007	CHB008	6.8	218.62	143.47	NS
6650	Niigata, Japan	2004	KNG013	6.63	216.69	89.32	NS

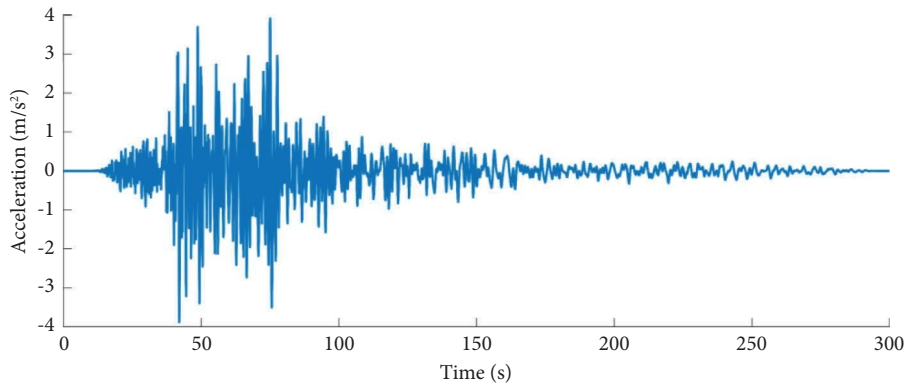


FIGURE 13: A typical earthquake record at a soft soil site (RSN-5295, Chuetsu-oki, Japan, PGA = 0.4 g).

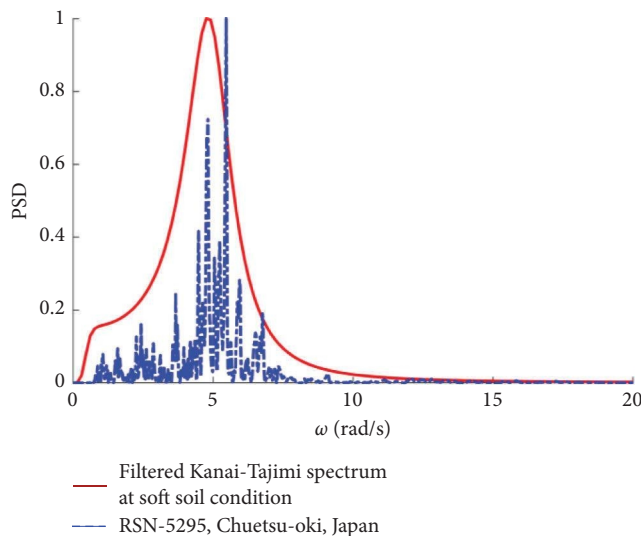


FIGURE 14: Comparison of the normalized filtered Kanai-Tajimi spectrum and the PSDs of the earthquake records at the soft soil sites.

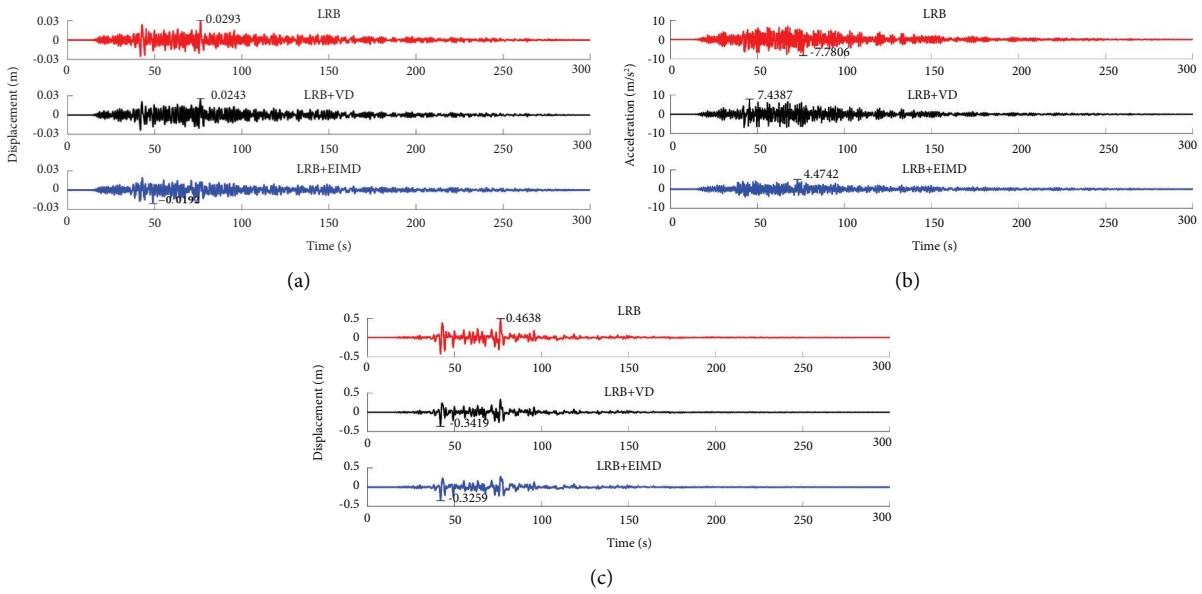


FIGURE 15: Comparison of the seismic responses of the three cases subjected to the RSN-5295 earthquake record. (a) Interstory drift at the first floor of the superstructure. (b) Absolute acceleration at the roof. (c) Base floor deformation.

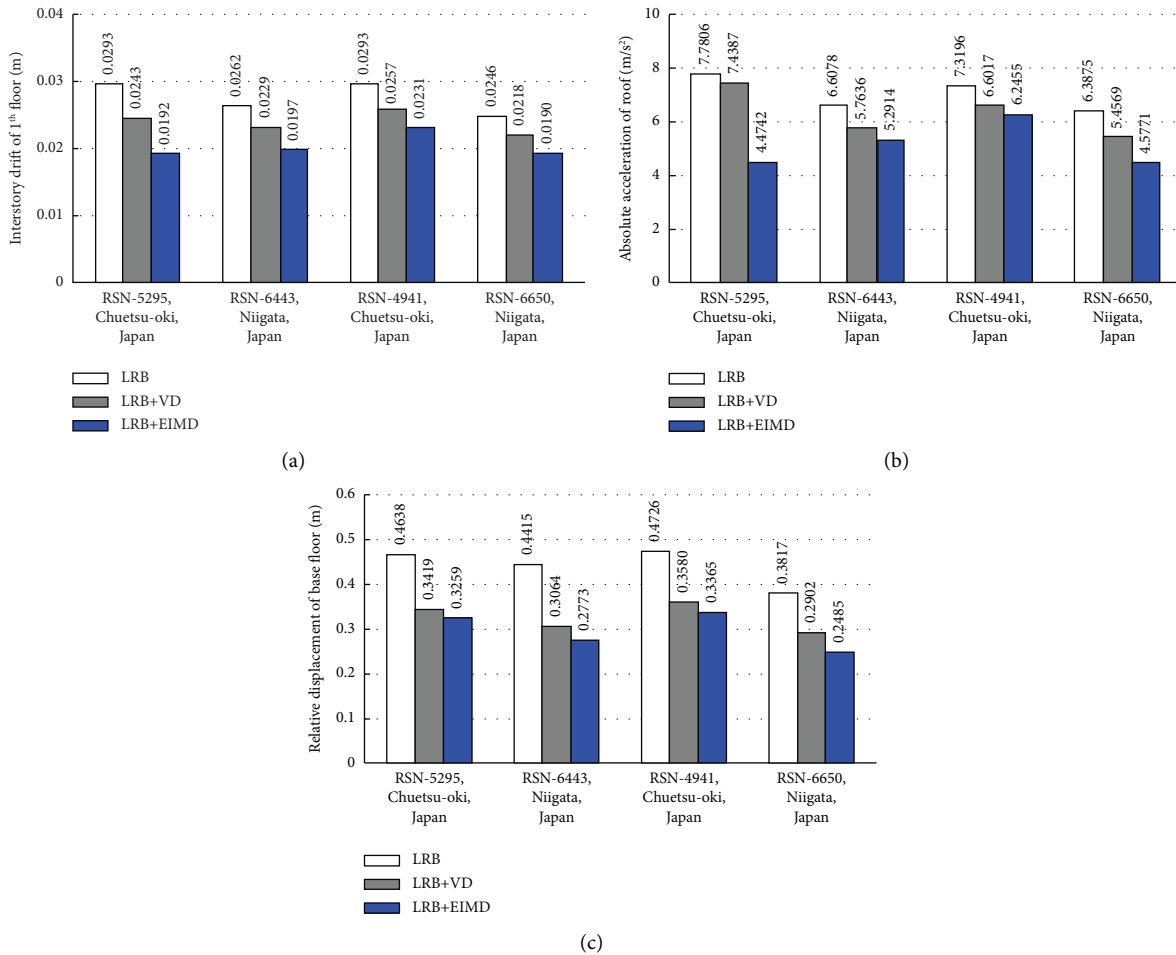


FIGURE 16: Comparison of the control performances of the EIMD and VD for the seven-story LRB-isolated building subjected to earthquake records (PGA = 0.4g). (a) Interstory drift at the first floor of the superstructure. (b) Absolute acceleration at the roof. (c) Base floor deformation.

Figure 16 shows the numerical results of the seismic response of the structure under the ground motion records, which illustrate that the optimal EIMD significantly enhances the seismic performance of the LRB-isolated structure.

5. Conclusions

The nonlinear stochastic analysis of a structure with a hybrid base isolation system consisting of the LRB and the EIMD has been conducted in the time domain through the state-space method. Taking the nonlinear behavior of the LRB into account, we derive the semianalytical solutions of the response variances of the 2-DOF base-isolated model subjected to the Kanai-Tajimi earthquake model. A stochastic optimization procedure is proposed for the EIMD parameters to minimize the interstory drift of the superstructure using the semi-analytical solutions. Using the optimization procedure, a comprehensive parametric study has been conducted to investigate the influence of the postyielding to preyielding stiffness ratio of the LRB and soil conditions on the optimal EIMD and its corresponding seismic control performance. In addition, the optimization procedure was applied to a seven-story LRB-isolated building, and a nonlinear seismic response analysis was conducted considering both artificial accelerograms and earthquake records. The following are the major conclusions that can be drawn from this study:

- (1) The optimal inertance-to-mass ratio μ increases with increasing the postyielding to preyielding stiffness ratio α . It is noted that the period of the BIS shortens with increasing the α . In other words, a more stiff system requires a larger inertance coefficient of the EIMD to further enlarge the system period and enhance the seismic performance.
- (2) The soil condition has a significant effect on the hybrid base isolation system with the EIMD. It is found that the hybrid base isolation system has better seismic performance in soft soil conditions than in firm soil conditions. The optimal inertance-to-mass ratio μ and optimal damping ratio ξ of the EIMD are larger at the soft soil site than their counterparts at the firm soil site. In soft soil conditions, the long-period components dominate the earthquake ground motions. Therefore, it requires a large μ to further prolong the system period, thus avoiding resonance response.
- (3) Numerical results illustrate that the EIMD outperforms the VD at the soft soil site. Considering the artificial seismic excitations, the performance enhancement by the EIMD compared with the VD for the base floor deformation, the interstory drift of the superstructure, and the superstructure acceleration are 3.2%, 17.5%, and 23.3%, respectively. When considering earthquake records compared with the VD cases, the performance enhancement by the EIMD for the above three responses is 6.4%, 12.5%, and 16.0%, respectively. Consequently, it is demonstrated that the hybrid base isolation system using the novel EIMD is promising

and that its performance can be improved compared with that of the conventional VD.

Data Availability

The data supporting the findings of this study are available from the authors upon request.

Conflicts of Interest

The authors declare that they have no conflicts of interest.

Authors' Contributions

Heng Wang handled methodology, investigation, data curation, and writing the original draft; Wenai Shen was in charge of conceptualization, methodology, project administration, supervision, resources, reviewing and editing the manuscript; Hongping Zhu was in charge of project administration, supervision, and resources; and Hui Luo handled project administration and supervision.

Acknowledgments

This study was jointly supported by the grants from the National Natural Science Foundation of China (grant nos. 51838006 and 52278309) and the National Key R&D Program of China (grant no. 2021YFF0501003).

References

- [1] J. M. Kelly, *Earthquake-resistant Design with Rubber*, Springer-Verlag, London, UK, 1993.
- [2] W. H. Robinson, "Lead-rubber hysteretic bearings suitable for protecting structures during earthquakes," *Seismic Isolation and Protective Systems*, vol. 2, no. 1, pp. 5–19, 2011.
- [3] R. S. Jangid, "Stochastic response of building frames isolated by lead-rubber bearings," *Structural Control and Health Monitoring*, vol. 17, no. 1, pp. 1–22, 2010.
- [4] D. M. Fenz and M. C. Constantinou, "Spherical sliding isolation bearings with adaptive behavior: Experimental verification," *Earthquake Engineering & Structural Dynamics*, vol. 37, no. 2, pp. 185–205, 2008.
- [5] T. A. Morgan and S. A. Mahin, "Achieving reliable seismic performance enhancement using multi-stage friction pendulum isolators," *Earthquake Engineering & Structural Dynamics*, vol. 39, no. 13, pp. 1443–1461, 2010.
- [6] C. S. Tsai, W. S. Chen, T. C. Chiang, and B. J. Chen, "Component and shaking table tests for full-scale multiple friction pendulum system," *Earthquake Engineering & Structural Dynamics*, vol. 35, no. 13, pp. 1653–1675, 2006.
- [7] Y. Li, S. Li, and Z. Chen, "Optimal design and effectiveness evaluation for inerter-based devices on mitigating seismic responses of base isolated structures," *Earthquake Engineering and Engineering Vibration*, vol. 20, no. 4, pp. 1021–1032, 2021.
- [8] D. Pietrosanti, M. De Angelis, and A. Giaralis, "Experimental seismic performance assessment and numerical modelling of nonlinear inerter vibration absorber (IVA)-equipped base isolated structures tested on shaking table," *Earthquake Engineering and Structural Dynamics*, vol. 50, no. 10, pp. 2732–2753, 2021.

- [9] L. Y. Cao and C. X. Li, "A high performance hybrid passive base-isolated system," *Structural Control and Health Monitoring*, vol. 29, no. 3, p. e2887, 2022.
- [10] N. U. Islam and R. S. Jangid, "Optimum parameters and performance of negative stiffness and inerter based dampers for base-isolated structures," *Bulletin of Earthquake Engineering*, pp. 1–28, 2022.
- [11] R. S. Jangid, "Performance and optimal design of base-isolated structures with clutching inerter damper," *Structural Control and Health Monitoring*, vol. 29, no. 9, Article ID e3000, 2022.
- [12] J. M. Kelly, "The role of damping in seismic isolation," *Earthquake Engineering and Structural Dynamics*, vol. 28, no. 1, pp. 3–20, 1999.
- [13] H. Wang, W. Shen, Y. M. Li, H. P. Zhu, and S. Y. Zhu, "Dynamic behavior and seismic performance of base-isolated structures with electromagnetic inertial mass dampers: analytical solutions and simulations," *Engineering Structures*, vol. 246, Article ID 113072, 2021.
- [14] K. Ikago, K. Saito, and N. Inoue, "Seismic control of single-degree-of-freedom structure using tuned viscous mass damper," *Earthquake Engineering and Structural Dynamics*, vol. 41, no. 3, pp. 453–474, 2012.
- [15] X. J. Yang, Y. Lei, L. J. Liu, H. P. Zhu, and W. Shen, "Two-step online identification of in-service cable-inertial mass damper systems under nonstationary wind excitations," *Mechanical Systems and Signal Processing*, vol. 187, Article ID 109940, 2023.
- [16] H. P. Zhu, Y. M. Li, W. Shen, and S. Y. Zhu, "Mechanical and energy-harvesting model for electromagnetic inertial mass dampers," *Mechanical Systems and Signal Processing*, vol. 120, pp. 203–220, 2019.
- [17] I. F. Lazar, S. A. Neild, and D. J. Wagg, "Using an inerter-based device for structural vibration suppression," *Earthquake Engineering and Structural Dynamics*, vol. 43, no. 8, pp. 1129–1147, 2014.
- [18] A. Giaralis and F. Petrini, "Wind-induced vibration mitigation in tall buildings using the tuned mass-damper-inerter," *Journal of Structural Engineering*, vol. 143, no. 9, Article ID 04017127, 2017.
- [19] W. Shen, Z. T. Long, L. Cai et al., "An inerter-based electromagnetic damper for civil structures: modeling, testing, and seismic performance," *Mechanical Systems and Signal Processing*, vol. 173, Article ID 109070, 2022.
- [20] K. Ye, S. Shu, L. Hu, and H. P. Zhu, "Analytical solution of seismic response of base-isolated structure with supplemental inerter," *Earthquake Engineering and Structural Dynamics*, vol. 48, no. 9, pp. 1083–1090, 2019.
- [21] M. Saitoh, "On the performance of gyro-mass devices for displacement mitigation in base isolation systems," *Structural Control and Health Monitoring*, vol. 19, no. 2, pp. 246–259, 2012.
- [22] H. Wang, W. Shen, H. P. Zhu, F. Kong, and S. Y. Zhu, "Stochastic seismic analysis of base-isolated structures with electromagnetic inertial mass dampers considering different soil conditions," *Bulletin of Earthquake Engineering*, vol. 473, pp. 1–26, 2021.
- [23] S. Nakaminami, K. Ikago, N. Inoue, and H. Kida, "Response characteristics of a base-isolated structure incorporated with a force-restricted viscous mass damper," in *Proceedings of the 15th World Conference on Earthquake Engineering*, Lisbon, Portugal, September, 2012.
- [24] Z. Chen, K. Junya, I. Masahiro, I. Kohju, and I. Norio, "Viscoelastically supported viscous mass damper incorporated into a seismic isolation system," *Journal of Earthquake and Tsunami*, vol. 10, no. 03, Article ID 1640009, 2016.
- [25] H. X. Sun, L. Zuo, X. Y. Wang, J. Peng, and W. X. Wang, "Exact H_2 optimal solutions to inerter-based isolation systems for building structures," *Structural Control and Health Monitoring*, vol. 26, no. 6, Article ID e2357, 2019.
- [26] D. De Domenico, N. Impollonia, and G. Ricciardi, "Soil-dependent optimum design of a new passive vibration control system combining seismic base isolation with tuned inerter damper," *Soil Dynamics and Earthquake Engineering*, vol. 105, pp. 37–53, 2018.
- [27] R. S. Jangid, "Optimum tuned inerter damper for base-isolated structures," *Journal of Vibration Engineering Technologies*, vol. 9, no. 7, pp. 1483–1497, 2021.
- [28] D. De Domenico and G. Ricciardi, "Optimal design and seismic performance of tuned mass damper inerter (TMDI) for structures with nonlinear base isolation systems," *Earthquake Engineering and Structural Dynamics*, vol. 47, no. 12, pp. 2539–2560, 2018.
- [29] Z. Zhao, R. F. Zhang, Y. Jiang, and C. Pan, "Seismic response mitigation of structures with a friction pendulum inerter system," *Engineering Structures*, vol. 193, pp. 110–120, 2019.
- [30] C. X. Li, K. Chang, L. Y. Cao, and Y. Huang, "Performance of a nonlinear hybrid base isolation system under the ground motions," *Soil Dynamics and Earthquake Engineering*, vol. 143, Article ID 106589, 2021.
- [31] H. Wang, W. Shen, H. Zhu, W. Wei, F. Kong, and S. Y. Zhu, "Performance enhancement of FPS-isolated buildings using an inerter-based damper: stochastic seismic analysis and optimization," *Mechanical Systems and Signal Processing*, vol. 177, Article ID 109237, 2022.
- [32] M. Shinozuka and G. Deodatis, "Simulation of stochastic processes by spectral representation," *Applied Mechanics Reviews*, vol. 44, no. 4, pp. 191–204, 1991.
- [33] T. I. Hsu and M. C. Bernard, "A random process for earthquake simulation," *Earthquake Engineering and Structural Dynamics*, vol. 6, no. 4, pp. 347–362, 1978.
- [34] European Committee for Standardization (Cen), *Eurocode 8. Design of Structures for Earthquake Resistance—Part 1: General Rules, Seismic Actions and Rules for Buildings*, European Committee for Standardization (CEN), Brussels, Belgium, 2004.